

Completion as Enhancement: A Degradation-Aware Selective Image Guided Network for Depth Completion

Zhiqiang Yan, Zhengxue Wang, Kun Wang, Jun Li[†], and Jian Yang[†]
Nanjing University of Science and Technology, China

Abstract

In this paper, we introduce the *Selective Image Guided Network (SigNet)*, a novel degradation-aware framework that transforms depth completion into depth enhancement for the first time. Moving beyond direct completion using convolutional neural networks (CNNs), SigNet initially densifies sparse depth data through non-CNN densification tools to obtain coarse yet dense depth. This approach eliminates the mismatch and ambiguity caused by direct convolution over irregularly sampled sparse data. Subsequently, SigNet redefines completion as enhancement, establishing a self-supervised degradation bridge between the coarse depth and the targeted dense depth for effective RGB-D fusion. To achieve this, SigNet leverages the implicit degradation to adaptively select high-frequency components (e.g., edges) of RGB data to compensate for the coarse depth. This degradation is further integrated into a multi-modal conditional Mamba, dynamically generating the state parameters to enable efficient global high-frequency information interaction. We conduct extensive experiments on the NYUv2, DIML, SUN RGBD, and TOFDC datasets, demonstrating the state-of-the-art (SOTA) performance of SigNet.

1. Introduction

Depth completion [27, 38, 40, 48, 51] aims to predict a dense depth map from sparse and noisy depth measurements, often using the corresponding RGB image for auxiliary guidance. The resulting dense depth map can benefit various downstream applications such as scene reconstruction [36, 39, 47] and autonomous driving [22, 45, 50].

The key challenges of this task lie in the sparse depth input data [21, 38, 40, 49, 51]. We summarize these challenges as mismatch and ambiguity. As shown in Fig. 1, the mismatch is caused by the irregularly sampled sparse depth with varying point distributions, while convolutions are spatially invariant with fixed kernel shapes. Moreover, it is ambiguous for convolutions to distinguish between valid and invalid depth measurements since unknown pixels in the sparse depth are recognized as zero.

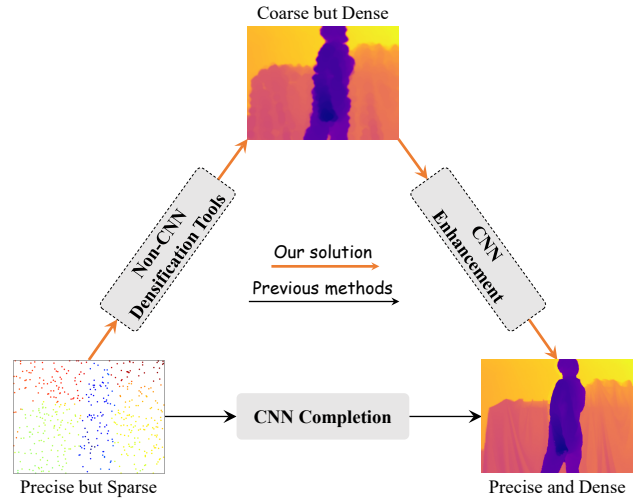


Figure 1. Illustration of our main concept. It redefines depth completion as depth enhancement. We first transform sparse depth input via non-CNN densification tools [14, 15], yielding coarse but dense depth. Then we predict the precise and dense depth from the coarse depth by leveraging degradation assumption [43, 59, 62].

To address these challenges, several excellent methods [21, 38, 40] have been proposed. For instance, SparseConvS [40] proposes sparsity invariant CNNs that explicitly model the location of missing data. To avoid directly convolving on sparse depth, Liu et al. [21] employs kernels learned by differentiable kernel regression layers to interpolate sparse data. BpNet [38] develops bilateral propagation, where the coefficients are generated based on both radiometric difference and spatial distance. These data-driven schemes are robust and impressive. However, they still cannot fully avoid the application of convolution on incomplete depth data, even though the depth data has become denser.

In this paper, our objective is to develop a novel solution that not only completely resolves the issues of mismatch and ambiguity but also provides a fresh perspective on revisiting the traditional depth completion task.

To this end, we propose a novel framework called the Selective Image Guided Network (SigNet). As depicted in Fig. 1, SigNet redefines depth completion as depth en-

hancement¹. It first leverages non-CNN densification tools [14, 15] to obtain coarse but dense depth. This coarse depth is then enhanced by a CNN-based subnetwork. Inspired by previous approaches [59, 62], we assume that there exists unknown degradation \mathbf{h} between the coarse depth \mathbf{Z} and the target depth \mathbf{Y} , described as

$$\mathbf{Z} = \mathbf{h}\mathbf{Y} + \mathbf{n}, \quad (1)$$

where \mathbf{n} denotes additive noise. Therefore, we can establish a connection between the source depth and the target depth through the degradation. A fundamental observation is that degradation typically occurs near edges, suggesting that this phenomenon can be leveraged to enhance RGB-D fusion. This is particularly relevant given that the coarse depth often lacks significant edge details, while the RGB image contains abundant high-frequency components. Specifically, SigNet introduces a Degradation-Aware Decomposition and Fusion (DADF) module. DADF begins by decomposing the implicit degradation \mathbf{h} into multiple patches and estimating their coefficients in the discrete cosine domain. Each patch is then used to adaptively select the most representative high-frequency information from the RGB image. To achieve effective RGB-D aggregation, DADF incorporates a conditional Mamba to encode long-range correlations. Unlike the vanilla Vision Mamba [25], which calculates state parameters from the input, DADF uses the degradation patches as additional conditions to generate the state parameters. This approach enables further global high-frequency information interaction.

In summary, our contributions are as follows:

- We introduce a novel framework called SigNet, which redefines depth completion as depth enhancement for the first time. By adopting a degradation-aware approach, SigNet not only offers a new perspective to the field but also fully eliminates the traditional challenges such as mismatch and ambiguity.
- We propose a Degradation-Aware Decomposition and Fusion (DADF) module. Utilizing degradation decomposition, DADF adaptively selects high-frequency components of RGB data to compensate for coarse depth. Furthermore, DADF achieves effective RGB-D fusion by incorporating conditional Mamba, where the state parameters are generated from degradation patches.
- We evaluate SigNet through comprehensive experiments on the NYUv2, DIML, SUN RGBD, and TOFDC datasets. The experimental results demonstrate the superiority of SigNet over previous SOTA approaches.

¹Specifically depth super-resolution (DSR). Mainstream DSR methods restore target depth directly from upsampled depth. Consequently, the processes and the end goals of depth completion and DSR are identical, *i.e.*, predicting clear depth from the same-resolution coarse depth.

2. Related Work

2.1. Depth Completion

Since the introduction of sparsity invariant CNNs by SparseConvs [40] to address missing depth data, the task of depth completion has garnered significant public attention. Generally, depth completion can be broadly categorized into two frameworks: depth-only and image-guided.

Depth-only methods [9, 12, 14, 28, 40, 41, 44, 51] obtain dense depth directly from a single sparse depth input. For instance, IP-Basic [14] designs reasonable combinations of basic image processing operations to densify sparse depth without using CNNs. Ma et al. [28] employ a UNet-like architecture to progressively densify the sparse depth input. FusionNet [41] designs a lightweight completion network that aggregates both global and local information with confidence adjustment. Moreover, Lu et al. [26] introduce a color image branch as auxiliary supervision during training.

Despite the advancements in single-modal methods, their effectiveness is often constrained without supplementary reference information. To address this challenge, numerous image-guided techniques have been proposed [11, 16, 19, 22, 37, 38, 45, 51, 53, 61, 64]. For instance, GuideNet [37] and RigNet [48] utilize color images to generate adaptive filtering kernels for depth feature extraction. FCFRNet [22] employs an energy-based fusion strategy to merge RGB-D modalities. GFormer [32] and CFormer [61] integrate convolution and transformer mechanisms to capture both local and global representations. LRRU [44] introduces a dynamic kernel scope that transitions from large to small to capture varying dependencies. FuseNet [3] and PointDC [56] incorporate LiDAR point cloud branches to model 3D geometries. BEV@DC [64] leverages a point-voxel architecture based on a bird’s-eye view to achieve a balance between effectiveness and efficiency. Additionally, DepthPrompting [30] proposes to embed priors of large depth models for better sensor-agnostic generalization.

To further advance completion models, spatial propagation networks (SPNs) have been introduced. The initial SPN [23] is designed to learn a pairwise similarity matrix. CSPN [5] applies this technique to depth completion by conducting recursive convolutions with fixed local neighborhood kernels, while CSPN++ [7] adapts by learning variable kernel sizes. PENet [11] expands the receptive fields using dilated convolutions. Furthermore, NLSPN [29] integrates non-local neighbors through deformable convolutions. DySPN [20] generates dynamic non-linear neighbors using an attention mechanism. Most recently, 3D SPNs [6] have been developed to encode 3D geometry. For instance, GraphCSPN [24] employs additional geometric constraints to regulate 3D propagation. TPVD [51] introduces a geometric SPN that constructs the affinity in 2D tri-perspective view spaces and their combined 3D projection space.

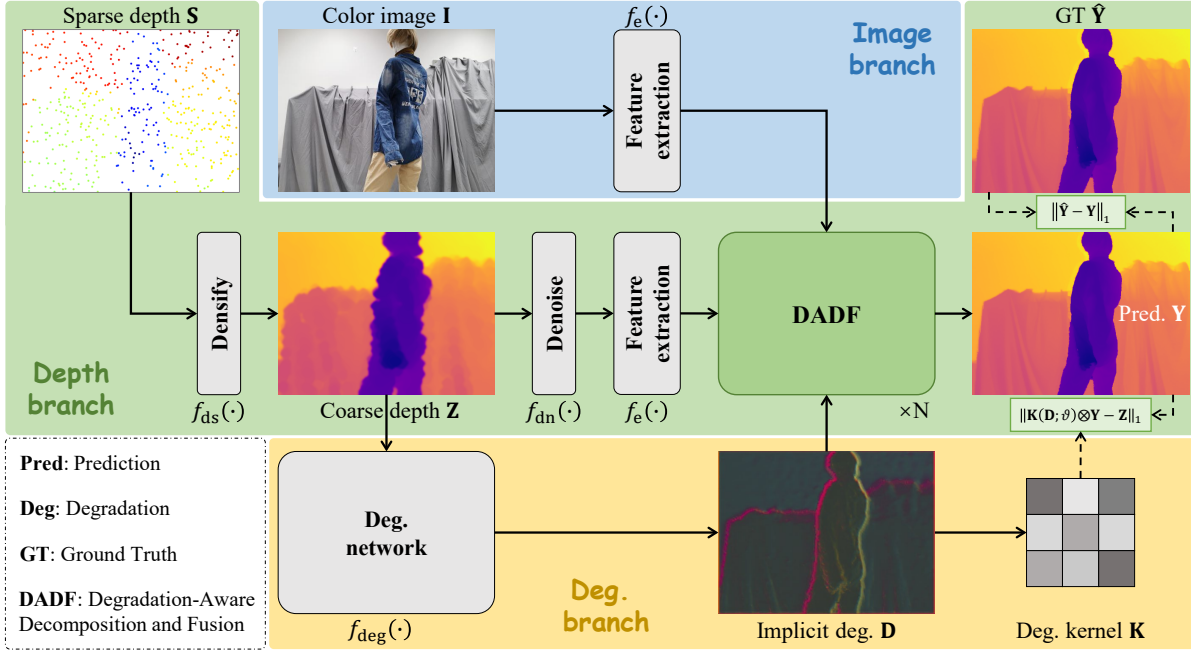


Figure 2. Pipeline of SigNet. The sparse depth data is initially filled to create a coarse depth map. We then utilize the degradation assumption in Eq. (1) to establish a connection between this coarse map and the target prediction. The color image features and degradation representations are employed to guide the multi-modal fusion through our proposed DADF module, as depicted in Fig. 3.

2.2. Degradation Learning

Recently, the development of color image restoration has been significantly propelled by advancements in degradation representations [43, 55, 59]. For instance, Zhang et al. [59] have constructed a sophisticated yet practical degradation model to simulate real-world image degradation for blind image super-resolution. Leveraging meta-learning, they also devised an implicit degradation estimator to model the degradation of low-resolution input, thereby guiding the restoration of high-resolution images. Similarly, Zhou et al. [63] estimate degradation for each local image region and propose a degradation-adaptive regression filter for blind super-resolution. Liang et al. [18] present a degradation-adaptive model that specifies the network parameters by estimating the degradation. Furthermore, several comprehensive image restoration methods [17, 57, 58] have been explored to address multiple forms of degradation simultaneously. For example, Zhang et al. [57] developed a multi-degradation image restoration network that incrementally learns degradation representations through clustering, without prior knowledge of the degradation information. Zhang et al. [58] build an ingredient-oriented degradation reformulation network to model the relationship among different images. Besides, Yao et al. [54] introduced a neural degradation representation learning method to capture latent features of degradation, which adaptively decomposes various types of degradation to enable comprehensive restoration.

3. Method

3.1. Overview

Fig. 2 shows our SigNet pipeline that consists of the depth branch, degradation branch, and image branch. In the depth branch, the sparse depth S is first filled via non-CNN densification tools [14, 15], obtaining a coarse depth map Z . According to Eq. (1), we employ denoising operators to weaken the negative impact of the noise n , yielding \hat{Z} . Then, we use residual groups [60] to extract features of the denoised depth \hat{Z} and the color image I in the image branch. In the degradation branch, The implicit degradation D is generated from a degradation network, where convolutions and residual groups are used. We thus utilize the image feature and degradation D to facilitate RGB-D fusion via our proposed Degradation-Aware Decomposition and Fusion (DADF). In summary, our SigNet redefines the depth completion as depth enhancement through the degradation assumption in Eq. (1), making the model free from the challenges of mismatch and ambiguity.

3.2. Task Switching

Degradation learning is widely utilized in the domain of low-level image restoration [43, 55, 59], achieving impressive performance. These image restoration tasks have two distinct characteristics: 1) the input and target data are usually dense, and 2) the resolution of the input data is

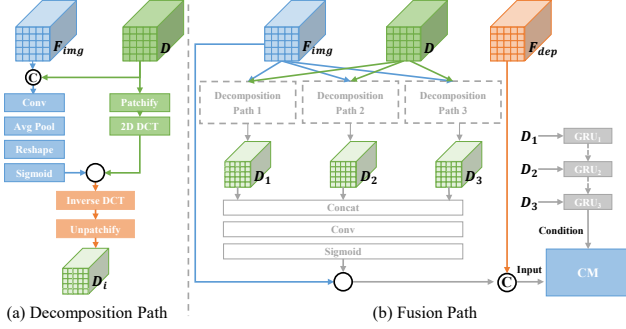


Figure 3. Overview of our DADF. CM: conditional Mamba.

lower than that of the target data. In practice, the low-resolution input data are typically upsampled using interpolation methods, such as bicubic interpolation. Consequently, the degradation matrix usually consists of a convolution whose kernel is derived from degradation representations and a downsampling function. In contrast, the depth completion task takes sparse depth data as input, and the resolutions of the input and target data are the same. Therefore, we aim to transform depth completion into depth enhancement by drawing an analogy between image restoration and depth completion.

As illustrated in Fig. 2, we first fill the sparse depth \mathbf{S} using non-CNN densification tools [14, 15] (denoted as $f_{ds}(\cdot)$), yielding a coarse but dense depth map \mathbf{Z}

$$\mathbf{Z} = f_{ds}(\mathbf{S}). \quad (2)$$

As discussed in Sec. 1, this approach eliminates the mismatch and ambiguity caused by direct convolution over irregularly sampled sparse data.

Then we employ a degradation network to estimate the implicit degradation \mathbf{D} . The degradation kernel \mathbf{K} is produced from \mathbf{D} using convolutions. Consequently, given the coarse depth \mathbf{Z} and target depth \mathbf{Y} and based on the analogy above, we can rewrite Eq. (1) as

$$\mathbf{Z} = \mathbf{K}(\mathbf{D}; \vartheta) \otimes \mathbf{Y} + \mathbf{n}, \quad (3)$$

where \otimes indicates convolution operation, ϑ is the network parameter. Since the resolutions are the same, our degradation equation does not need the downsampling function.

3.3. Degradation-Aware Decomposition and Fusion

As we know that degradation typically occurs near edges, suggesting that this cue can be leveraged to enhance RGB-D fusion, especially considering that the coarse depth often lacks significant edge details, while the RGB image contains abundant high-frequency components. Thus, we propose DADF that is shown in Fig. 3.

We use \mathbf{F}_{img} and \mathbf{F}_{dep} to denote the image feature and

Algorithm 1: Conditional SSM Block

Input: $\mathbf{F}_{rgb}, \{\mathbf{D}_i | i = 1, 2, 3\} : (HW, C)$

Output: $\hat{\mathbf{F}}_{rgb} : (HW, C)$

- 1 $\mathbf{A} : (C, N) \leftarrow \text{Parameter}_A$
 - 2 $\mathbf{B} : (HW, N) \leftarrow \text{Linear}_B(f_{gru}(\mathbf{F}_{rgb}, \{\mathbf{D}_i | i = 1, 2, 3\}))$
 - 3 $\mathbf{C} : (HW, N) \leftarrow \text{Linear}_C(f_{gru}(\mathbf{F}_{rgb}, \{\mathbf{D}_i | i = 1, 2, 3\}))$
 - 4 $\Delta : (HW, C) \leftarrow \log(1 + \exp(\text{Linear}_\Delta(f_{gru}(\mathbf{F}_{rgb}, \{\mathbf{D}_i | i = 1, 2, 3\}))) + \text{Parameter}_\Delta)$
 - 5 $\bar{\mathbf{A}} : (HW, C, N) \leftarrow \exp(\Delta \otimes \mathbf{A})$
 - 6 $\bar{\mathbf{B}} : (HW, C, N) \leftarrow \Delta \otimes \mathbf{B}$
 - 7 $\hat{\mathbf{F}}_{rgb} \leftarrow \text{SSM}(\bar{\mathbf{A}}, \bar{\mathbf{B}}, \mathbf{C})(\mathbf{F}_{rgb})$
 - 8 **return** $\hat{\mathbf{F}}_{rgb}$
-

depth feature, respectively.

$$\mathbf{F}_{img} = f_e(\mathbf{I}) \quad (4)$$

$$\mathbf{F}_{dep} = f_e(f_{dn}(\mathbf{Z})), \quad (5)$$

where $f_e(\cdot)$ and $f_{dn}(\cdot)$ refer to the feature extraction network and denoising function, severally.

As presented in Fig. 3, DADF takes as input the image feature \mathbf{F}_{img} , depth feature \mathbf{F}_{dep} , and degradation \mathbf{F}_D .

Decomposition. To obtain the most representative components of \mathbf{F}_D , we first transform it into frequency domain using discrete cosine transform (DCT). Then, we adaptively learn a spectrum mask and apply it to the decomposed frequency spectrum to effectively enhance the informative frequency bands and suppress irrelevant frequency bands. Finally, the frequency spectrum is transformed back to the spatial domain via inverse DCT. This step is described as

$$\{\mathbf{D}_i | i = 1, 2, 3\} = f_{dct}(\mathbf{D}). \quad (6)$$

We then utilize concatenation, convolution, pooling, and Sigmoid operators (denoted as $f_m(\cdot)$) to generate a mask m , which is multiplied with the combination of the frequency components to produce a new mask \hat{m} , adaptively selecting the representative image feature $\hat{\mathbf{F}}_{img}$. This process can be defined as

$$m = f_m(\mathbf{F}_{img}, \mathbf{D}), \quad (7)$$

$$\hat{m} = f_{idct}(m \cdot (f_{ac}(\sum_{i=1}^3 \mathbf{D}_i))), \quad (8)$$

$$\hat{\mathbf{F}}_{img} = \hat{m} \cdot \mathbf{F}_{img}, \quad (9)$$

where f_{idct} refers to inverse DCT and $f_{ac}(\cdot)$ represents the combination function of addition and convolutions.

Fusion. As a result, we further leverage the decomposed degradation \mathbf{D}_i to enable effective RGB-D fusion. It is well-known that Mamba [10] is good at handling long-range correlations. Inspired by recent Vision Mamba [25],

Dataset	Method	Params. (M) ↓	RMSE (mm) ↓	REL ↓	δ_1 (%) ↑	δ_2 (%) ↑	δ_3 (%) ↑	Venue
NYUv2	Bilateral [1]	-	532	0.132	85.1	93.5	95.9	CVPR 2005
	S2D [28]	26.1	230	0.054	94.5	97.3	98.9	ICRA 2019
	CSPN [4]	17.4	173	0.020	96.3	98.6	99.5	ECCV 2018
	DfuseNet [34]	-	156	0.016	98.8	99.7	99.9	ITSC 2019
	DM-LRN [33]	-	205	0.014	98.8	99.6	99.9	IROS 2021
	RDF-GAN [42]	-	139	0.013	98.7	99.6	99.9	CVPR 2022
	AGG-Net [2]	129.1	92	0.014	99.4	99.9	100.0	ICCV 2023
	BPNet [38]	89.9	88	0.011	99.6	99.9	100.0	CVPR 2024
	SigNet (ours)	3.3	83	0.012	99.7	99.9	100.0	-
DIML	Bilateral [1]	-	636	0.189	83.0	88.8	92.4	CVPR 2005
	CSPN [4]	17.4	162	0.033	96.1	98.7	99.6	ECCV 2018
	DfuseNet [34]	-	143	0.023	98.4	99.4	99.9	ITSC 2019
	DM-LRN [33]	-	149	0.015	99.0	99.6	99.9	IROS 2021
	AGG-Net [2]	129.1	78	0.011	99.6	99.9	100.0	ICCV 2023
	BPNet [38]	89.9	68	0.011	99.4	99.8	100.0	CVPR 2024
	SigNet (ours)	3.3	55	0.006	99.7	99.9	100.0	-
SUN RGBD	S2D [28]	26.1	329	0.074	93.9	97.0	98.1	ICRA 2019
	CSPN [4]	17.4	295	0.137	95.6	97.5	98.4	ECCV 2018
	DLiDAR [31]	53.4	279	0.061	96.9	98.0	98.4	CVPR 2019
	DM-LRN [33]	-	267	0.063	97.6	98.2	98.7	IROS 2021
	RDF-GAN [42]	-	255	0.059	96.9	98.4	99.0	CVPR 2022
	AGG-Net [2]	129.1	152	0.038	98.5	99.0	99.4	ICCV 2023
	BPNet [38]	89.9	124	0.025	98.9	99.4	99.8	CVPR 2024
	SigNet (ours)	3.3	116	0.022	99.0	99.4	99.8	-
TOFDC	CSPN [4]	17.4	224	0.042	94.5	95.3	96.5	ECCV 2018
	GuideNet [37]	73.5	146	0.030	97.6	98.9	99.5	TIP 2020
	PENet [11]	131.5	241	0.043	94.6	95.3	95.5	ICRA 2021
	NLSPN [29]	25.8	174	0.029	96.4	97.9	98.9	ECCV 2020
	CFormer [61]	83.5	113	0.029	99.1	99.6	99.9	CVPR 2023
	RigNet [48]	65.2	133	0.025	97.6	99.1	99.7	ECCV 2022
	GraphCSPN [24]	26.4	253	0.052	92.0	96.9	98.7	ECCV 2022
	PointDC [56]	25.1	109	0.021	98.5	99.2	99.6	ICCV 2023
	TPVD [51]	31.2	92	0.014	99.1	99.6	99.9	CVPR 2024
	SigNet (ours)	3.3	87	0.012	99.2	99.7	99.9	-

Table 1. Quantitative comparison on four depth completion datasets. The **best** and **suboptimal** results are highlighted. Note that most of the results on NYUv2, DIML, and SUN RGBD are borrowed directly from AGG-Net [2], while those of TOFDC are from TPVD [51].

we present a variant, *i.e.*, Conditional Mamba (CM). As shown in Fig. 3, the selected image feature $\hat{\mathbf{F}}_{img}$ and raw depth feature \mathbf{F}_{dep} are concatenated into CM, where the decomposed degradation \mathbf{D}_i serves as the condition:

$$\mathbf{F}_{rgb} = f_{cc}(\hat{\mathbf{F}}_{img}, \mathbf{F}_{dep}), \quad (10)$$

$$\hat{\mathbf{F}}_{rgb} = f_{cm}(\mathbf{F}_{rgb}, \{\mathbf{D}_i | i = 1, 2, 3\}), \quad (11)$$

where f_{cc} denotes the combination function of concatenation and convolutions, f_{cm} is the Condition Mamba function. As reported in Alg. 1, the state parameters \mathbf{B} and \mathbf{C} are calculated based on both the RGB-D input and degradation using gated recurrent convolution units.

3.4. Loss Function

As shown in our pipeline, the total loss function \mathcal{L}_t consists of a reconstruction loss \mathcal{L}_r and a self-supervised degradation learning loss \mathcal{L}_d .

For one pixel p in the valid pixel set \mathbb{P} of \mathbf{y} :

$$\begin{aligned} - \text{RMSE} & \quad \sqrt{\frac{1}{|\mathbb{P}|} \sum (\hat{\mathbf{y}}_p - \mathbf{y}_p)^2} \\ - \text{REL} & \quad \frac{1}{|\mathbb{P}|} \sum |\hat{\mathbf{y}}_p - \mathbf{y}_p| / \hat{\mathbf{y}}_p \\ - \delta_{1.25^i} & \quad \frac{|\mathbb{S}|}{|\mathbb{P}|}, \mathbb{S} : \max(\hat{\mathbf{y}}_p / \mathbf{y}_p, \mathbf{y}_p / \hat{\mathbf{y}}_p) < 1.25^i \end{aligned}$$

Table 2. Metric definition. \mathbf{y} : prediction, $\hat{\mathbf{y}}$: ground truth.

The reconstruction loss \mathcal{L}_r is defined as

$$\mathcal{L}_r = \frac{1}{N} \sum_{i=1}^N \|\hat{\mathbf{Y}}_i - \mathbf{Y}_i\|_1, \quad (12)$$

where N represents the number of training samples, and $\|\cdot\|_1$ denotes the L_1 norm. $\hat{\mathbf{Y}}$ and \mathbf{Y} are the ground truth depth and the predicted depth, respectively.

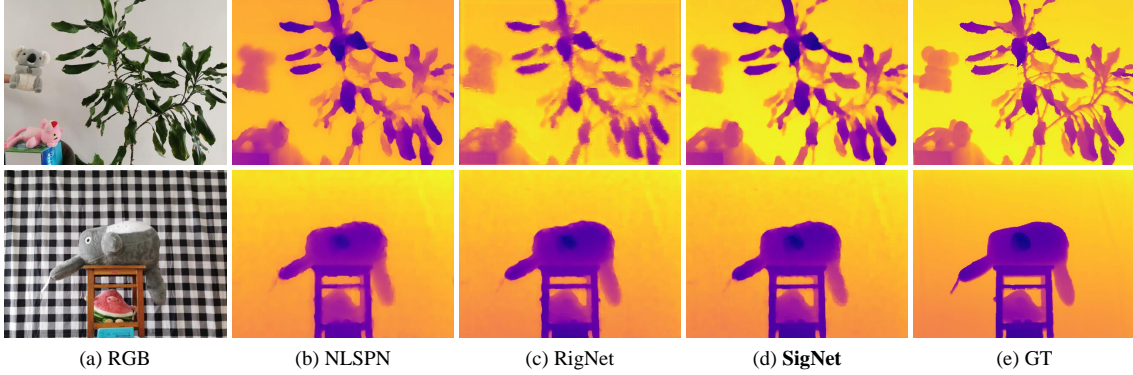


Figure 4. Visual comparison with SOTA methods on TOFDC dataset, including NLSPN [29], RigNet [48], and our SigNet.

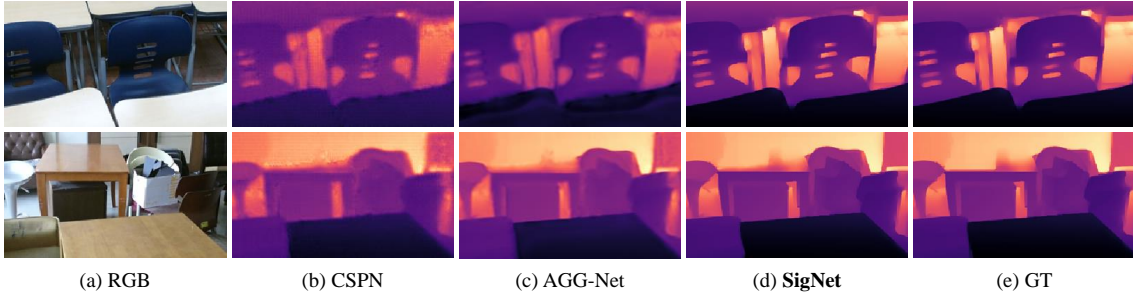


Figure 5. Visual comparison with SOTA methods on DIML dataset, including CSPN [4], AGG-Net [2], and our SigNet.

Then, we introduce the degradation loss \mathcal{L}_d to facilitate the degradation learning process:

$$\mathcal{L}_d = \frac{1}{N} \sum_{i=1}^N \|\mathbf{K} \otimes \mathbf{Y} - \mathbf{Z}\|_1, \quad (13)$$

where \mathbf{K} refers to the degradation kernel learned from the implicit degradation representation \mathbf{D} . \mathbf{Z} corresponds to the coarse depth. \otimes denotes the convolution operation, where \mathbf{K} serves as the convolution kernel.

As a result, the total training loss is defined as:

$$\mathcal{L}_t = \mathcal{L}_r + \lambda \mathcal{L}_d, \quad (14)$$

where λ is a hyper-parameter, empirically set to 0.1. By the constraint of the auxiliary loss \mathcal{L}_d , our model can build additional connect between the input and output, thus predicting more accurate depth results.

4. Experiment

4.1. Dataset

We evaluate our SigNet method on four popular datasets, including NYUv2, DIML, SUN RGBD, and TOFDC benchmarks. For NYUv2, DIML, and SUN RGBD, we maintain the settings used in AGG-Net [2], while for TOFDC, we follow the settings of TPVD [51].

NYUv2 [35] is the most commonly used dataset for depth completion, consisting of 1,449 sets from 464 different indoor scenes using Microsoft Kinect. AGG-Net divides this dataset into 420 images for training and 1,029 for testing. The initial resolution of the RGB-D pairs is 640×480 , which are randomly cropped and resized to 324×288 .

DIML [8] is a newly introduced dataset featuring a series of RGB-D frames captured by the Kinect V2 for indoor scenes and the ZED stereo camera for outdoor scenes. In addition to the usual invalid patterns, it includes numerous edge shadows and irregular holes, making it ideal for evaluating the adaptability of depth completion models to various invalid patterns. AGG-Net focuses solely on the indoor portion of the dataset, which comprises 1,609 RGB-D pairs for training and 503 pairs for testing. The resolution is randomly cropped and resized from 512×288 to 320×192 .

SUN RGB-D [36] is a comprehensive dataset containing 10,335 refined RGB-D pairs, captured using four different sensors across 19 major scene categories. According to the official scheme, the training set includes 4,845 pairs, while the testing set comprises 4,659 pairs. The resolution is randomly cropped and resized from 730×530 to 384×288 .

TOFDC [51] is collected using the time-of-flight (TOF) depth sensor and RGB camera of a Huawei P30 Pro, encompassing various scenes such as textures, flowers, bodies, and toys under different lighting conditions and in open spaces.

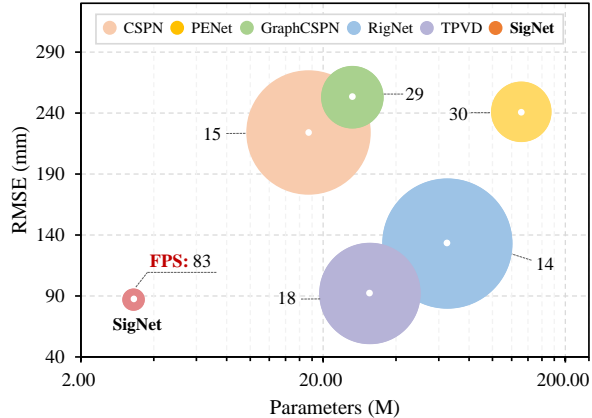


Figure 6. Complexity comparison on TOFDC dataset. Larger circle areas indicate faster inference speed.

It includes 10,000 RGB-D pairs of resolution 512×384 for training and 560 pairs for evaluation. The ground truth depth maps were captured by a Helios TOF camera.

4.2. Metric

Following previous works [2, 29, 31, 37, 51], the metrics include the Root Mean Squared Error (RMSE), Absolute Relative Error (REL), and Accuracy with Threshold $\delta_{1.25^i}$, where $i = 1, 2, 3$. Please see Tab. 2 for more details.

4.3. implementation Detail

We implement our SigNet on PyTorch using a single 3090 GPU. We train it for 20 epochs using the Adam optimizer [13] with the momentum parameters $\beta_1 = 0.9$ and $\beta_2 = 0.999$, a starting learning rate of 1×10^{-4} , and a weight decay of 1×10^{-6} . The balance coefficient γ in the loss function is set to 0.1. Additionally, to enhance the performance of our model, we employ random crop data augmentation and normalization during training.

4.4. Comparison with SOTA

To assess the effectiveness of our SigNet, we benchmark it against the traditional bilateral filtering method [1] and some recent SOTA deep learning approaches such as [2, 28, 29, 34, 38]. The error and accuracy results for the competing models are sourced from their original publications or obtained by retraining them following the default settings.

4.4.1. Performance Analysis

On NYUv2. As a widely used benchmark dataset, NYUv2 is often employed to evaluate the effectiveness of models. From the first row of Table 1, we can observe that SigNet achieves competitive performance on the NYUv2 dataset, with an RMSE that is $5mm$ lower than the second-best method. Additionally, although our method lags behind BPNet [38] by only 0.001 in the REL metric, SigNet significantly reduces the number of parameters by 96%.

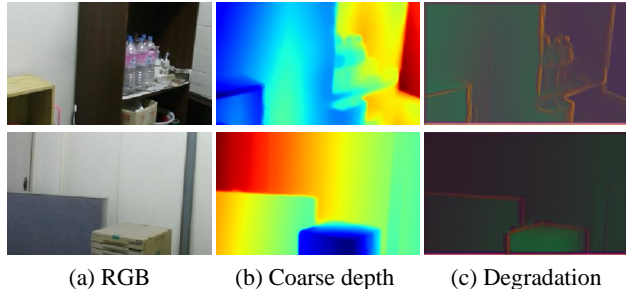


Figure 7. Visual examples of filled coarse depth maps and degradation representations on DIML dataset.

On DIML. DIML is collected from both indoor and outdoor scenes, suffering from severe edge shadows and irregular holes. Our method is implemented using the same experimental settings as previous approaches [2, 33]. As shown in the second row of Table 1, SigNet demonstrates the best performance across all evaluation metrics. For example, compared to the suboptimal model, our approach decreases the RMSE by 19% and the REL by 45%. Fig. 7 shows some degradation examples.

On SUN RGBD. The large-scale SUN RGB-D dataset is leveraged to evaluate the generalization capability of our SigNet across different sensors and scenes. Table 1 (third row) reveals that our method surpasses previous state-of-the-art approaches across all metrics. Notably, SigNet achieves an $8mm$ lower RMSE than the latest BPNet [38] and a $36mm$ lower RMSE compared to AGG-Net [2].

On TOFDC. TOFDC encompasses extensive data captured under various lighting conditions and in open spaces. It is utilized to further assess the performance of the proposed model. The quantitative results in the last row of Table 1 indicate that our method achieves state-of-the-art performance. Compared to the second-best TPVD [51], SigNet reduces the RMSE by $5mm$ and the REL by 0.002, while also decreasing the number of parameters by $27.9M$.

4.4.2. Visualization Analysis

Figs. 4 and 5 respectively display the visual results on the TOFDC and DIML datasets. We can discover that SigNet successfully recovers accurate and clear depth structures. For instance, compared to previous models, the leaves in Fig. 4 and the chair in Fig. 5 predicted by our method are sharper and closer to the ground-truth. Overall, these visual results demonstrate that our method effectively enhances the performance of depth completion.

4.4.3. Complexity Analysis

Fig. 6 shows that our method achieves an excellent balance among RMSE, parameters, FPS, and inference time. For example, compared to the fewer parameter CSPN [4], our SigNet not only reduces parameters by 81% and inference time by 82%, but also decreases RMSE by 61%. Additionally, our method surpasses the latest TPVD [51] with a 5%

SigNet	Degradation Bridge		RGB-D Fusion				RMSE (mm)
	Densify	Denoise	Conc.	Att.	DADF-D	DADF-F	
i							108
ii	✓		✓				95
iii	✓		✓				92
iv	✓	✓		✓			74
v	✓	✓			✓		68
v	✓	✓			✓	✓	55

Table 3. Ablation study of our proposed SigNet on DIML dataset. Conc.: concat, Att.: attention, DADF-D: degradation decomposition in DADF module, DADF-F: conditional Mamba fusion.

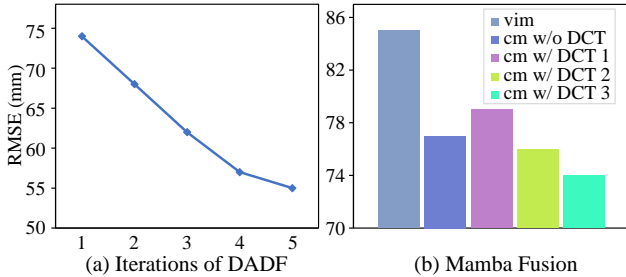


Figure 8. Ablation study of DADF on DIML dataset.

lower RMSE and 78% lower FPS, while reducing parameters by 89% and inference time by 78%.

4.5. Ablation Study

SigNet Designs. Table 3 presents the ablation results on the DIML test split. The iteration of DADF is set as five. SigNet-i serves as the baseline, where both the degradation bridge and DADF module are removed, and the RGB-D features are fused using addition. Building on this, SigNet-ii redefines depth completion as depth enhancement through densification and degradation, concatenating the RGB and degradation features, resulting in a 13 mm improvement. This highlights the superiority of our task transformation approach. Additionally, SigNet-iii incorporates a Gaussian denoising operator to further reduce error. To better utilize the degradation, SigNet-iv applies a Sigmoid function and element-wise multiplication to obtain an attention map, enabling adaptive selection of RGB features. Consequently, performance improves significantly from 92 mm to 74 mm. Furthermore, SigNet-v employs degradation-aware decomposition, reducing the error by an additional 6 mm. The results of SigNet-iii, iv, and v demonstrate the effectiveness of our adaptive feature selection strategy. Notably, in SigNet-iii, iv, and v, the selected RGB and depth features are encoded through concatenation and convolutions. Finally, with the introduction of our conditional Mamba, SigNet-vi surpasses SigNet-v by 13 mm in RMSE, representing a significant improvement. Overall, each component positively impacts the performance of the baseline.

Mamba Fusion and Iteration of DADF. Fig. 8 (a) illustrates the ablation study of Mamba fusion on the DIML

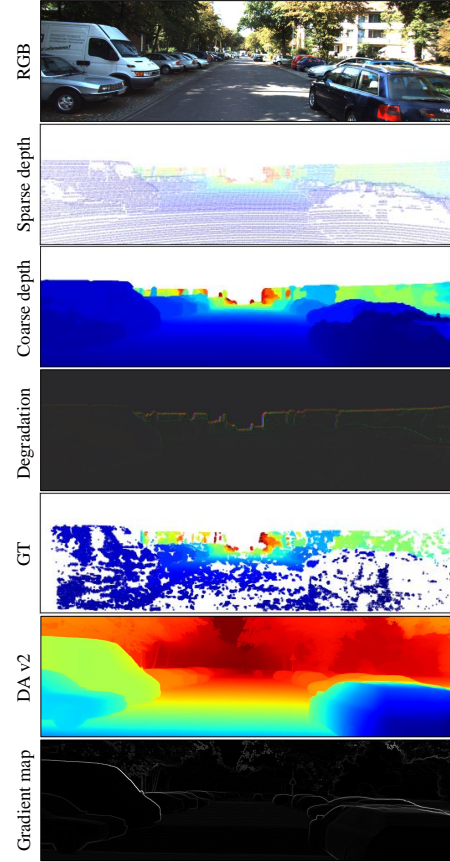


Figure 9. Visual results of failure cases on KITTI benchmark [40]. DA v2 denotes the large depth model DepthAnything v2 [52].

dataset. For rapid validation, we employ DADF only once. The baseline ViM directly encodes the combined RGB-D features using the vanilla Vision Mamba [25]. When we apply our Conditional Mamba with initial degradation and RGB-D features as input, the error decreases by 8 mm. Additionally, the introduction of degradation decomposition using DCT further enhances performance. We also observe that the results improve as the number of DCT components increases, highlighting the effectiveness of our gradual DCT decomposition design. Fig. 8 (b) presents the ablation study of our DADF with different iterations on the DIML dataset. We find that performance improves with an increasing number of iterations. For an optimal balance between efficiency and effectiveness, we set the final iteration count to five.

4.6. Failure Case

Our method is primarily evaluated in indoor scenes and some simple outdoor scenes with closer distances. By constraining dense predictions with coarse depth maps, SigNet can effectively predict their degradation representations. However, as depicted in Fig. 9, SigNet fails to estimate reasonable degradation on the outdoor KITTI benchmark [40]. We identify two main reasons for this:

1) The ground truth depth maps of KITTI are very sparse, with only about 30% valid pixels. This sparsity leads to inconsistent depth edges, resulting in a relatively weak constraint. For instance, the degradation in Fig. 9 even introduces some initial LiDAR lines.

2) The depth distances of KITTI data are much larger, which significantly weaken edge details. As observed, the degradation in Fig. 9 can only learn very coarse and blurry representations near edges at short range, while at long range, it learns incorrect representations.

One potential solution is to provide the model with supervisory signals regarding dense contents and precise edges. It is well-known that large depth models can produce dense depth with impressive sharp edges. For example, we employ DepthAnything v2 [52] to generate the corresponding dense depth. We discover that the edges of cars and even tree leaves are much clearer. Although the depth scale does not match that of KITTI, we can generate a map that offers constraints near edges via gradient or boundary extraction techniques [46]. Certainly, the results of DepthAnything v2 [52] or DepthAnything v2 itself can also be utilized to facilitate depth completion, warranting further exploration.

5. Conclusion

In this paper, we redefined depth completion as depth enhancement for the first time with our novel framework, SigNet. SigNet leveraged non-CNN densification tools to transform sparse depth data into coarse yet dense depth, fully eliminating the mismatch and ambiguity caused by direct convolution over irregularly sampled sparse data. More importantly, by establishing a self-supervised degradation bridge, SigNet effectively fused RGB-D data. It utilized degradation decomposition to dynamically select high-frequency components of RGB and build a conditional Mamba for the depth enhancement. Extensive experiments validated the superiority of SigNet, highlighting its potential for depth related applications.

References

- [1] Antoni Buades, Bartomeu Coll, and J-M Morel. A non-local algorithm for image denoising. In *CVPR*, pages 60–65, 2005. 5, 7
- [2] Dongyue Chen, Tingxuan Huang, Zhimin Song, Shizhuo Deng, and Tong Jia. Agg-net: Attention guided gated-convolutional network for depth image completion. In *ICCV*, pages 8853–8862, 2023. 5, 6, 7
- [3] Yun Chen, Bin Yang, Ming Liang, and Raquel Urtasun. Learning joint 2d-3d representations for depth completion. In *ICCV*, pages 10023–10032, 2019. 2
- [4] Xinjing Cheng, Peng Wang, and Ruigang Yang. Learning depth with convolutional spatial propagation network. In *ECCV*, pages 103–119, 2018. 5, 6, 7
- [5] Xinjing Cheng, Peng Wang, and Ruigang Yang. Depth estimation via affinity learned with convolutional spatial propagation network. In *ECCV*, pages 103–119, 2018. 2
- [6] Xinjing Cheng, Peng Wang, and Ruigang Yang. Learning depth with convolutional spatial propagation network. *IEEE Transactions on Pattern Analysis and Machine Intelligence*, 42(10):2361–2379, 2019. 2
- [7] Xinjing Cheng, Peng Wang, Chenye Guan, and Ruigang Yang. Cspn++: Learning context and resource aware convolutional spatial propagation networks for depth completion. In *AAAI*, pages 10615–10622, 2020. 2
- [8] Jaehoon Cho, Dongbo Min, Youngjung Kim, and Kwanghoon Sohn. A large rgb-d dataset for semi-supervised monocular depth estimation. *arXiv preprint arXiv:1904.10230*, 2019. 6
- [9] Abdelrahman Eldesokey, Michael Felsberg, and Fahad Shahbaz Khan. Confidence propagation through cnns for guided sparse depth regression. *IEEE Transactions on Pattern Analysis and Machine Intelligence*, 42(10):2423–2436, 2020. 2
- [10] Albert Gu and Tri Dao. Mamba: Linear-time sequence modeling with selective state spaces. *arXiv preprint arXiv:2312.00752*, 2023. 4
- [11] Mu Hu, Shuling Wang, Bin Li, Shiyu Ning, Li Fan, and Xiaojin Gong. Penet: Towards precise and efficient image guided depth completion. In *ICRA*, 2021. 2, 5
- [12] Maximilian Jaritz, Raoul De Charette, Emilie Wirbel, Xavier Perrotton, and Fawzi Nashashibi. Sparse and dense data with cnns: Depth completion and semantic segmentation. In *3DV*, pages 52–60, 2018. 2
- [13] Diederik P Kingma and Jimmy Ba. Adam: A method for stochastic optimization. In *Computer Ence*, 2014. 7
- [14] Jason Ku, Ali Harakeh, and Steven L Waslander. In defense of classical image processing: Fast depth completion on the cpu. In *CRV*, pages 16–22, 2018. 1, 2, 3, 4
- [15] Anat Levin, Dani Lischinski, and Yair Weiss. Colorization using optimization. In *SIGGRAPH*, pages 689–694, 2004. 1, 2, 3, 4
- [16] Ang Li, Zejian Yuan, Yonggen Ling, Wanchao Chi, Chong Zhang, et al. A multi-scale guided cascade hourglass network for depth completion. In *WACV*, pages 32–40, 2020. 2
- [17] Boyun Li, Xiao Liu, Peng Hu, Zhongqin Wu, Jiancheng Lv, and Xi Peng. All-in-one image restoration for unknown corruption. In *CVPR*, pages 17452–17462, 2022. 3
- [18] Jie Liang, Hui Zeng, and Lei Zhang. Efficient and degradation-adaptive network for real-world image super-resolution. In *ECCV*, pages 574–591, 2022. 3
- [19] Yuankai Lin, Tao Cheng, Qi Zhong, Wending Zhou, and Hua Yang. Dynamic spatial propagation network for depth completion. In *AAAI*, pages 1638–1646, 2022. 2
- [20] Yuankai Lin, Hua Yang, Tao Cheng, Wending Zhou, and Zhouping Yin. Dyspn: Learning dynamic affinity for image-guided depth completion. *IEEE Transactions on Circuits and Systems for Video Technology*, pages 1–1, 2023. 2
- [21] Lina Liu, Yiyi Liao, Yue Wang, Andreas Geiger, and Yong Liu. Learning steering kernels for guided depth completion. *IEEE Transactions on Image Processing*, 30:2850–2861, 2021. 1

- [22] Lina Liu, Xibin Song, Xiaoyang Lyu, Junwei Diao, Mengmeng Wang, Yong Liu, and Liangjun Zhang. Fcfr-net: Feature fusion based coarse-to-fine residual learning for depth completion. In *AAAI*, pages 2136–2144, 2021. 1, 2
- [23] Sifei Liu, Shalini De Mello, Jinwei Gu, Guangyu Zhong, Ming-Hsuan Yang, and Jan Kautz. Learning affinity via spatial propagation networks. In *NeurIPS*, 2017. 2
- [24] Xin Liu, Xiaofei Shao, Bo Wang, Yali Li, and Shengjin Wang. Graphcspn: Geometry-aware depth completion via dynamic gcns. In *ECCV*, pages 90–107. Springer, 2022. 2, 5
- [25] Yue Liu, Yunjie Tian, Yuzhong Zhao, Hongtian Yu, Lingxi Xie, Yaowei Wang, Qixiang Ye, and Yunfan Liu. Vmamba: Visual state space model. *arXiv preprint arXiv:2401.10166*, 2024. 2, 4, 8
- [26] Kaiyue Lu, Nick Barnes, Saeed Anwar, and Liang Zheng. From depth what can you see? depth completion via auxiliary image reconstruction. In *CVPR*, pages 11306–11315, 2020. 2
- [27] Fangchang Ma and Sertac Karaman. Sparse-to-dense: Depth prediction from sparse depth samples and a single image. In *ICRA*, pages 4796–4803. IEEE, 2018. 1
- [28] Fangchang Ma, Guilherme Venturini Cavalheiro, and Sertac Karaman. Self-supervised sparse-to-dense: Self-supervised depth completion from lidar and monocular camera. In *ICRA*, 2019. 2, 5, 7
- [29] Jinsun Park, Kyungdon Joo, Zhe Hu, Chi-Kuei Liu, and In So Kweon. Non-local spatial propagation network for depth completion. In *ECCV*, 2020. 2, 5, 6, 7
- [30] Jin-Hwi Park, Chanhwi Jeong, Junoh Lee, and Hae-Gon Jeon. Depth prompting for sensor-agnostic depth estimation. In *CVPR*, pages 9859–9869, 2024. 2
- [31] Jiexiong Qiu, Zhaopeng Cui, Yinda Zhang, Xingdi Zhang, Shuaicheng Liu, Bing Zeng, and Marc Pollefeys. Deeplidar: Deep surface normal guided depth prediction for outdoor scene from sparse lidar data and single color image. In *CVPR*, pages 3313–3322, 2019. 5, 7
- [32] Kyeongha Rho, Jinsung Ha, and Youngjung Kim. Guideformer: Transformers for image guided depth completion. In *CVPR*, pages 6250–6259, 2022. 2
- [33] Dmitry Senushkin, Mikhail Romanov, Ilia Belikov, Nikolay Patakin, and Anton Konushin. Decoder modulation for indoor depth completion. In *IROS*, pages 2181–2188. IEEE, 2021. 5, 7
- [34] Shreyas S Shivakumar, Ty Nguyen, Ian D Miller, Steven W Chen, Vijay Kumar, and Camillo J Taylor. Dfusetnet: Deep fusion of rgb and sparse depth information for image guided dense depth completion. In *ITSC*, pages 13–20. IEEE, 2019. 5, 7
- [35] Nathan Silberman, Derek Hoiem, Pushmeet Kohli, and Rob Fergus. Indoor segmentation and support inference from rgb-d images. In *ECCV*, pages 746–760. Springer, 2012. 6
- [36] Shuran Song, Samuel P Lichtenberg, and Jianxiong Xiao. Sun rgb-d: A rgb-d scene understanding benchmark suite. In *CVPR*, pages 567–576, 2015. 1, 6
- [37] Jie Tang, Fei-Peng Tian, Wei Feng, Jian Li, and Ping Tan. Learning guided convolutional network for depth completion. *IEEE Transactions on Image Processing*, 30:1116–1129, 2020. 2, 5, 7
- [38] Jie Tang, Fei-Peng Tian, Boshi An, Jian Li, and Ping Tan. Bilateral propagation network for depth completion. In *CVPR*, pages 9763–9772, 2024. 1, 2, 5, 7
- [39] Diego Thomas and Akihiro Sugimoto. A flexible scene representation for 3d reconstruction using an rgb-d camera. In *ICCV*, pages 2800–2807, 2013. 1
- [40] Jonas Uhrig, Nick Schneider, Lukas Schneider, Uwe Franke, Thomas Brox, and Andreas Geiger. Sparsity invariant cnns. In *3DV*, pages 11–20, 2017. 1, 2, 8
- [41] Wouter Van Gansbeke, Davy Neven, Bert De Brabandere, and Luc Van Gool. Sparse and noisy lidar completion with rgb guidance and uncertainty. In *MVA*, pages 1–6, 2019. 2
- [42] Haowen Wang, Mingyuan Wang, Zhengping Che, Zhiyuan Xu, Xiuquan Qiao, Mengshi Qi, Feifei Feng, and Jian Tang. Rgb-depth fusion gan for indoor depth completion. In *CVPR*, pages 6209–6218, 2022. 5
- [43] Longguang Wang, Yingqian Wang, Xiaoyu Dong, Qingyu Xu, Jungang Yang, Wei An, and Yulan Guo. Unsupervised degradation representation learning for blind super-resolution. In *CVPR*, pages 10581–10590, 2021. 1, 3
- [44] Yufei Wang, Bo Li, Ge Zhang, Qi Liu, Tao Gao, and Yuchao Dai. Lrru: Long-short range recurrent updating networks for depth completion. In *ICCV*, pages 9422–9432, 2023. 2
- [45] Yufei Wang, Ge Zhang, Shaoqian Wang, Bo Li, Qi Liu, Le Hui, and Yuchao Dai. Improving depth completion via depth feature upsampling. In *CVPR*, pages 21104–21113, 2024. 1, 2
- [46] Zhengxue Wang, Zhiqiang Yan, and Jian Yang. Sgnet: Structure guided network via gradient-frequency awareness for depth map super-resolution. In *AAAI*, pages 5823–5831, 2024. 9
- [47] Zhiqiang Yan, Xiang Li, Kun Wang, Zhenyu Zhang, Jun Li, and Jian Yang. Multi-modal masked pre-training for monocular panoramic depth completion. In *ECCV*, pages 378–395, 2022. 1
- [48] Zhiqiang Yan, Kun Wang, Xiang Li, Zhenyu Zhang, Jun Li, and Jian Yang. Rignet: Repetitive image guided network for depth completion. In *ECCV*, pages 214–230, 2022. 1, 2, 5, 6
- [49] Zhiqiang Yan, Kun Wang, Xiang Li, Zhenyu Zhang, Jun Li, and Jian Yang. Desnet: Decomposed scale-consistent network for unsupervised depth completion. In *AAAI*, pages 3109–3117, 2023. 1
- [50] Zhiqiang Yan, Yupeng Zheng, Kun Wang, Xiang Li, Zhenyu Zhang, Shuo Chen, Jun Li, and Jian Yang. Learnable differencing center for nighttime depth perception. *arXiv preprint arXiv:2306.14538*, 2023. 1
- [51] Zhiqiang Yan, Yuankai Lin, Kun Wang, Yupeng Zheng, Yufei Wang, Zhenyu Zhang, Jun Li, and Jian Yang. Tri-perspective view decomposition for geometry-aware depth completion. In *CVPR*, pages 4874–4884, 2024. 1, 2, 5, 6, 7
- [52] Lihe Yang, Bingyi Kang, Zilong Huang, Zhen Zhao, Xiaogang Xu, Jiashi Feng, and Hengshuang Zhao. Depth anything v2. *arXiv preprint arXiv:2406.09414*, 2024. 8, 9
- [53] Yanchao Yang, Alex Wong, and Stefano Soatto. Dense depth posterior (ddp) from single image and sparse range. In *CVPR*, pages 3353–3362, 2020. 2

- [54] Mingde Yao, Ruikang Xu, Yuanshen Guan, Jie Huang, and Zhiwei Xiong. Neural degradation representation learning for all-in-one image restoration. *IEEE Transactions on Image Processing*, 2024. 3
- [55] Guanghao Yin, Wei Wang, Zehuan Yuan, Wei Ji, Dongdong Yu, Shouqian Sun, Tat-Seng Chua, and Changhu Wang. Conditional hyper-network for blind super-resolution with multiple degradations. *IEEE Transactions on Image Processing*, 31:3949–3960, 2022. 3
- [56] Zhu Yu, Zehua Sheng, Zili Zhou, Lun Luo, Si-Yuan Cao, Hong Gu, Huaqi Zhang, and Hui-Liang Shen. Aggregating feature point cloud for depth completion. In *ICCV*, pages 8732–8743, 2023. 2, 5
- [57] Cheng Zhang, Yu Zhu, Qingsen Yan, Jinqiu Sun, and Yan-ning Zhang. All-in-one multi-degradation image restoration network via hierarchical degradation representation. In *ACM MM*, pages 2285–2293, 2023. 3
- [58] Jinghao Zhang, Jie Huang, Mingde Yao, Zizheng Yang, Hu Yu, Man Zhou, and Feng Zhao. Ingredient-oriented multi-degradation learning for image restoration. In *CVPR*, pages 5825–5835, 2023. 3
- [59] Kai Zhang, Jingyun Liang, Luc Van Gool, and Radu Timofte. Designing a practical degradation model for deep blind image super-resolution. In *ICCV*, pages 4791–4800, 2021. 1, 2, 3
- [60] Yulun Zhang, Kunpeng Li, Kai Li, Lichen Wang, Bineng Zhong, and Yun Fu. Image super-resolution using very deep residual channel attention networks. In *ECCV*, pages 286–301, 2018. 3
- [61] Youmin Zhang, Xianda Guo, Matteo Poggi, Zheng Zhu, Guan Huang, and Stefano Mattoccia. Completionformer: Depth completion with convolutions and vision transformers. In *CVPR*, pages 18527–18536, 2023. 2, 5
- [62] Zhiwei Zhong, Xianming Liu, Junjun Jiang, Debin Zhao, and Xiangyang Ji. Guided depth map super-resolution: A survey. *ACM Computing Surveys*, 55(14s):1–36, 2023. 1, 2
- [63] Hongyang Zhou, Xiaobin Zhu, Jianqing Zhu, Zheng Han, Shi-Xue Zhang, Jingyan Qin, and Xu-Cheng Yin. Learning correction filter via degradation-adaptive regression for blind single image super-resolution. In *ICCV*, pages 12365–12375, 2023. 3
- [64] Wending Zhou, Xu Yan, Yinghong Liao, Yuankai Lin, Jin Huang, Gangming Zhao, Shuguang Cui, and Zhen Li. Bev@dc: Bird’s-eye view assisted training for depth completion. In *CVPR*, pages 9233–9242, 2023. 2